COMMUNICATION

Active Control of Ferroelectric Switching Using Defect-Dipole Engineering

*Daesu Lee, Byung Chul Jeon, Seung Hyub Baek, Sang Mo Yang, Yeong Jae Shin, Tae Heon Kim, Yong Su Kim, Jong-Gul Yoon, Chang Beom Eom, and Tae Won Noh**

Electrical switching of spontaneous polarization in ferroelectric materials offers a means of designing a broad range of multifunctional devices.[1–3] Ferroelectric switching is universally governed by defects.[3,4] Active control of the defect structures, therefore, has the potential for furthering utilization of ferroelectric materials and advancing novel applications. Here, we demonstrate active control of the defect dipole structure and associated polarization switching in a ferroelectric $BiFeO_3$ thin film without compromising its ferroelectric properties. We visualize the unique functionality of the defect dipoles to control local polarization switching. Also, by actively controlling the defect dipoles, we systematically vary the macroscopic polarization-voltage (P–V) hysteresis loop in a capacitor geometry, commonly used in real device applications. These results provide a foundation for novel device design utilizing ferroelectric materials, such as high-density multilevel data storage memories.

Ferroelectric materials have emerged as a primary functional building block for a wide spectrum of electronic, energy-storage, and information-technology devices.[1–3] These ferroelectric applications come from fast, reversible switching between thermodynamically equivalent spontaneous polarization states under an applied electric field. The polarization switching is also strongly coupled to other material properties, such as electronic,[5–7] magnetic,[8,9] optical,[10] and chemical[11] properties, enabling multifunctional devices. Thus, the development and utilization of ferroelectric devices depend critically on our ability to control field-induced polarization switching as we want. However, such precise control is quite difficult because polarization switching is a stochastic and complicated process, occurring via the nucleation and growth of domains.[4,12,13]

Dr. D. Lee, B. C. Jeon, Dr. S. M. Yang, Y. J. Shin, Dr. T. H. Kim, Dr. Y. S. Kim, Prof. T. W. Noh
IBS-Center for Functional Interfaces of Correlated Electron Systems
and Department of Physics and Astronomy
Seoul National University
Seoul 151-747, Korea
E-mail: twnoh@snu.ac.kr
Prof. J.-G. Yoon
Department of Physics
University of Suwon
Suwon, Gyunggi-do 445-743, Korea
Prof. C. B. Eom, Dr. S. H. Baek
Department of Materials Science and Engineering
University of Wisconsin-Madison
Madison, Wisconsin 53706, USA

DOI: 10.1002/adma.201203101

Defect engineering has played a crucial role in the rapid development of modern semiconductor devices because it has provided powerful methods for controlling their physical properties and resulting functionality. As in semiconductor devices, defect engineering has the potential to enhance the functionality of ferroelectric devices; we can control ferroelectric properties, such as a P–V hysteresis loop, by modifying the polarization-switching process with defects. Note that defects affect the thermodynamic stability of ferroelectric polarization and can act as nucleation centers for polarization switching, as well as pinning sites for moving domain walls. Furthermore, typical ferroelectric materials, such as perovskite titanates, allow for a diversity of point defects (e.g., oxygen vacancies) and extended defects. The recent emergence of scanning probe microscopy and transmission electron microscopy-based techniques has expedited defect studies in ferroelectric materials.[12–15] Previous studies, however, have focused on how polarization switching is affected by the given defects. Very little effort has been directed toward actively controlling the defect structure and the associated polarization switching.

In this study, we demonstrate the active control of irreversible defect dipoles (D_{defect})[3] in ferroelectric $BiFeO_3$ thin film without compromising its ferroelectric properties. D_{defect} is defined as an electric dipole consisting of charged defects, and D_{defect} in our film is probably composed of Bi vacancy and oxygen vacancy. It is well known that parallel alignment of the D_{defect} along the polarization direction (i.e., $D_{defect}//P_S$) is energetically favored.[16–20] This dipolar interaction between D_{defect} and P_S enables us to actively control the D_{defect} structure, as schematically depicted in **Figure 1**a. Initially, we write a polarization domain pattern as we want, and then we anneal the written domain pattern at temperatures below the Curie temperature. During the annealing process, the D_{defect} realigns to the energetically favored state of $D_{defect}//P_S$ by thermal migration of the point defects (e.g., oxygen vacancies).[18,21,22] The resulting D_{defect} structure would become the same as that of the intentionally written domain pattern. We visualize that the controlled D_{defect} structure can be used to control local polarization switching using piezoresponse force microscopy (PFM). Furthermore, using the controlled D_{defect} structures, we artificially generate macroscopic double-polarization switching (Figure 1b), in which the intermediate polarization (P_{int}) and switching voltage (V_{SW}) can be varied systematically. Finally, we suggest a possible real application for high-density multilevel data storage using our concept.

We first changed the downward-polarized domain of the as-grown $BiFeO_3$ film to a square bi-domain pattern (**Figure 2**a).

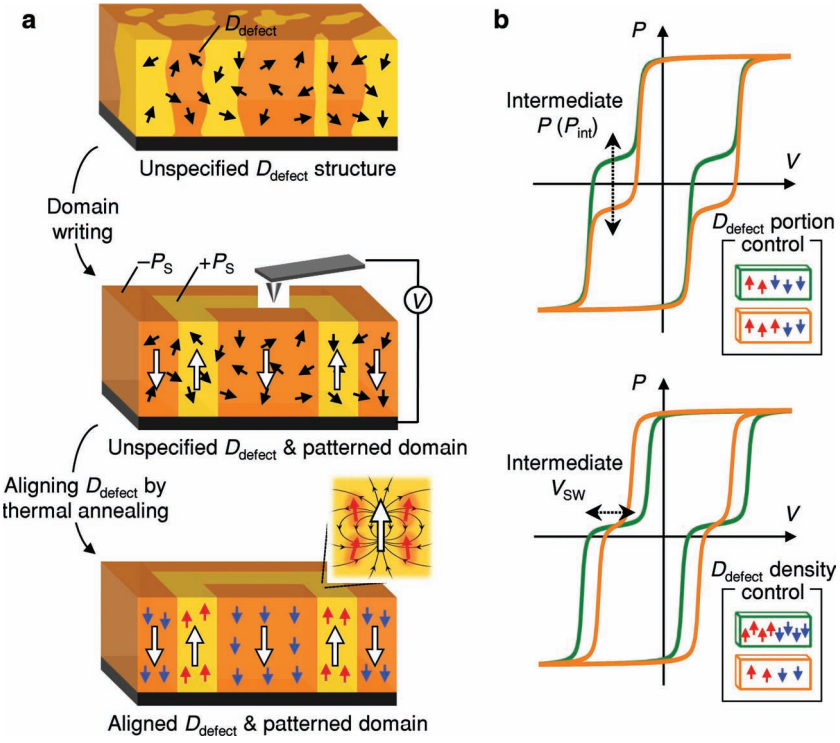

Figure 1. Active control of D_{defect} and associated ferroelectric switching. a) A scheme to control the D_{defect} structure. Partial domain writing and subsequent thermal annealing allow the active control of the D_{defect} structure. b) Double-polarization switching generated by the effect of D_{defect}. According to the portion of upward and downward D_{defect}, we can vary the intermediate polarization (P_{int}) value. Also, according to the density of aligned D_{defect}, we can vary the intermediate switching voltage (V_{SW}). V_{SW} is defined as the threshold voltage for making the P_{int} state.

The polarization in a 10-μm × 10-μm region of the film was switched to the upward state (i.e., $+P_S$) by scanning the film surface with a tip biased with a voltage of –12.5 V that exceeded the coercive voltage for the film. Then, the polarization within a square area of 5 μm × 5 μm in the center was switched back to the downward state (i.e., $-P_S$) by applying a bias of +12.5 V to the tip. Specifically for the parameters of our study, we were concerned only with the out-of-plane component of the polarization, and $+P_S$ ($-P_S$) indicates the upward (downward) out-of-plane saturated polarization state. After the domain-writing process, we read the written domain pattern by PFM (Supporting Information, Figure S2), and then annealed the sample at 300 °C for 40 min. The first panel in Figure 2a shows the domain pattern after annealing, as measured by PFM.

We found that the prepared domain pattern in the $BiFeO_3$ thin films was robust against thermal annealing. Its pattern was mostly preserved even after annealing (Figure 2a and Supporting Information, Figure S2); this may be due to the high Curie temperature and large coercive field of the film.[23–25] With the surface capped by a top electrode, the domains became much more robust, with little change at high temperature (Supporting Information, Figure S3). A previous study reported the presence of D_{defect} in our as-grown $BiFeO_3$ films.[19] The annealing process can align the D_{defect} along the P_S orientation in the prepared domain structure. As a result of annealing, the regions of (A) and (A)′ in the first panel of Figure 2a are expected to exclusively have the downward D_{defect}, whereas the (B) region is expected to include only the upward D_{defect}. Thus, the annealing-based method enables us to actively control the D_{defect} structure (i.e., the location and portion of the upward or downward D_{defect}). Such a controlled D_{defect} structure would affect the overall

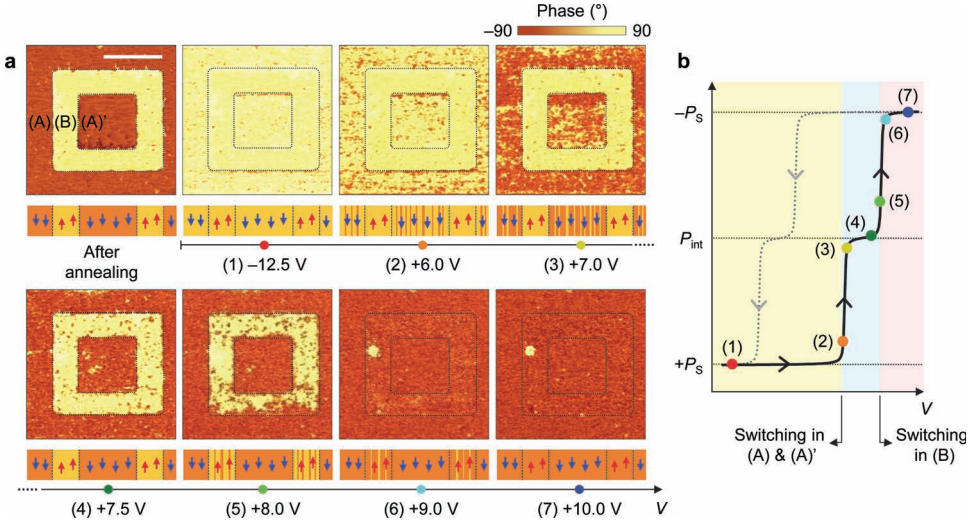

Figure 2. Visualization of the D_{defect} effects on local domain evolution. a) A chronological out-of-plane PFM phase-image series during polarization switching from $+P_S$ to $-P_S$ state in the annealed region. Scale bar represents 5 μm. b) Overall polarization switching under the influence of D_{defect}.

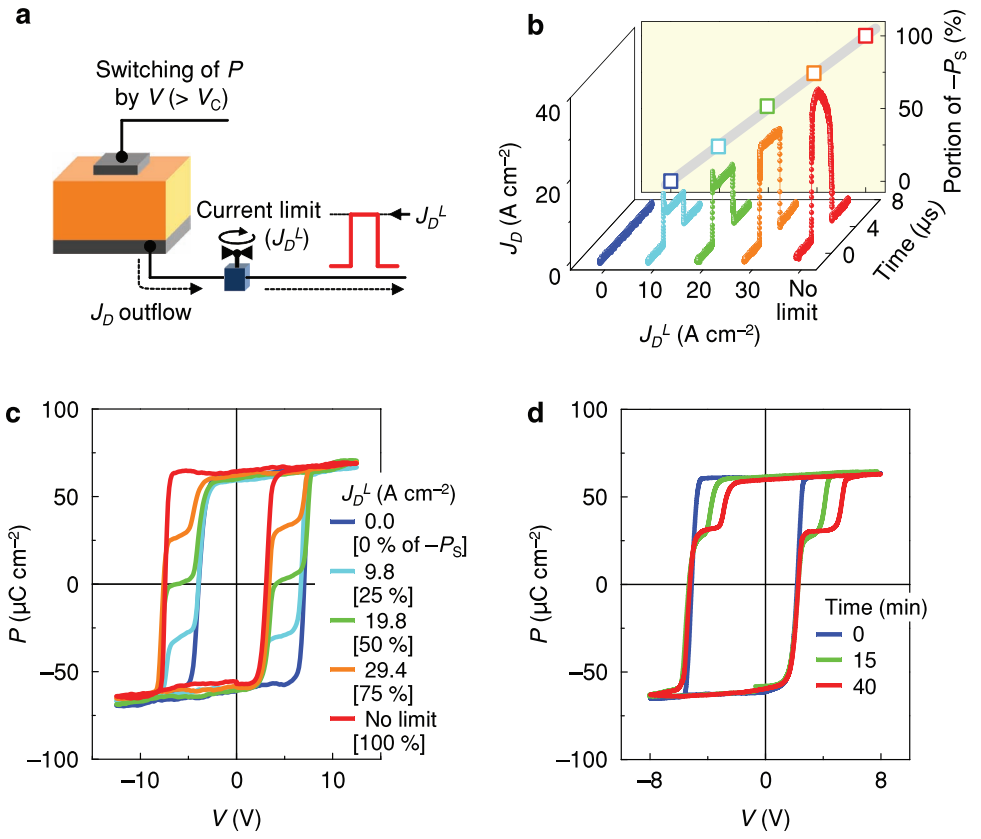

Figure 3. Control of the macroscopic polarization switching in the capacitor geometry. a) A schematic diagram for the precise control of polarization by limiting J_D. b) Plots of outflowing current generated from J_D during polarization switching, according to the J_D^L values. c) A systematic variation in P_{int} in P–V loops after portion control of D_{defect}. We control the D_{defect} portion by annealing the capacitor, where we precisely determine the $+P_S/-P_S$ domain portion as a function of J_D^L. d) A systematic variation in V_{SW} in the P–V loops after the density control of D_{defect}. We control the density of the aligned D_{defect} by adjusting the annealing time.

polarization-switching behavior significantly (Supporting Information, Figure S4).

To visualize the correlation between the controlled D_{defect} structure and local domain evolution, we used a PFM technique.[26–28] After thermal annealing, we poled the whole domain region into the $+P_S$ state by applying a negative probe-tip bias of –12.5 V (second panel in Figure 2a). Then, we monitored the polarization reversal to the $-P_S$ state by applying an incrementally increasing positive bias. When we applied a tip bias of +6.0 V, nucleation and growth of small domains began only in the (A) and (A)′ regions. Interestingly, even after applying a +7.0 V tip bias, the (B) region remained almost unswitched, whereas most of the (A) and (A)′ regions were switched to the $-P_S$ state. The (B) region began to switch just after the application of a 7.5 V tip bias, and it had switched completely to the $-P_S$ state as the tip bias approached +10 V. This means that the polarization switching to the $-P_S$ state was facilitated in the (A) and (A)′ regions by the downward D_{defect}, but was impeded in the (B) region by the upward D_{defect}. Figure 2b schematically summarizes the overall polarization switching under the influence of D_{defect}. The effect of the D_{defect} stabilized the mixed domain pattern over a certain voltage range (corresponding to (3) and (4) in Figure 2b), providing an additional stable state (i.e., P_{int}).

Most ferroelectric devices for electronic applications have a capacitor geometry in which the top ferroelectric surface is covered with a conducting electrode. For such applications, we cannot use the local switching technique with PFM, so we need other reliable methods to control the D_{defect} precisely in the capacitor geometry. Recently, we devised a convenient way to write a precise portion of $+P_S$ and $-P_S$ domains in the capacitor geometry.[29,30] In this technique,[29] the displacement current, J_D, is kept below J_D^L during polarization switching, as schematically shown in **Figure 3**a. J_D^L is defined as an upper limit on the current outflow. Because polarization switching is always accompanied by J_D, we can use it as a practical tuning parameter in controlling the portion of $+P_S/-P_S$ domains. By annealing our $BiFeO_3$ film with a predetermined portion of $+P_S/-P_S$ domains, we can obtain a sample that has precisely determined portions of upward and downward D_{defect} in the capacitor geometry.

We confirmed the feasibility of our capacitor geometry approach by measuring the macroscopic P–V hysteresis loops. By varying J_D^L during polarization switching (Figure 3b), we prepared five capacitors with $+P_S/-P_S$ domain portions of 100/0, 75/25, 50/50, 25/75, and 0/100. After manipulating the domain structure, we annealed the capacitors at 300 °C for 40 min. During this process, we expected the upward and downward

D_{defect} portions to follow the $+P_S/-P_S$ domain portions. After the annealing, we measured the P–V loops. The capacitor including only the upward (downward) D_{defect} showed the imprinted P–V loops shifted to the right (left) side, as shown in Figure 3c. In contrast, the capacitors with mixed upward/downward D_{defect} clearly showed the double P–V loops. According to the portions of upward and downward D_{defect}, the P_{int} values in the double P–V loops varied systematically.

In addition to the portion control, we controlled the degree of the D_{defect} alignment along P_S (i.e., the aligned D_{defect} density) by adjusting the annealing time. Once the annealing process was underway, the D_{defect} gradually aligned along the P_S direction by thermal rearrangement of the point defects (e.g., oxygen vacancies).[18] Thus, the degree of alignment increased with the annealing time, at some point reaching saturation. Figure 3d shows the changes in the P–V loops in the same capacitor after annealing for 15 and 40 min. We expected a lower degree of D_{defect} alignment along P_S after annealing for 15 min compared with the case when annealing for 40 min. The capacitor annealed for less time showed a smaller, less distinct modification in its corresponding P–V loop.

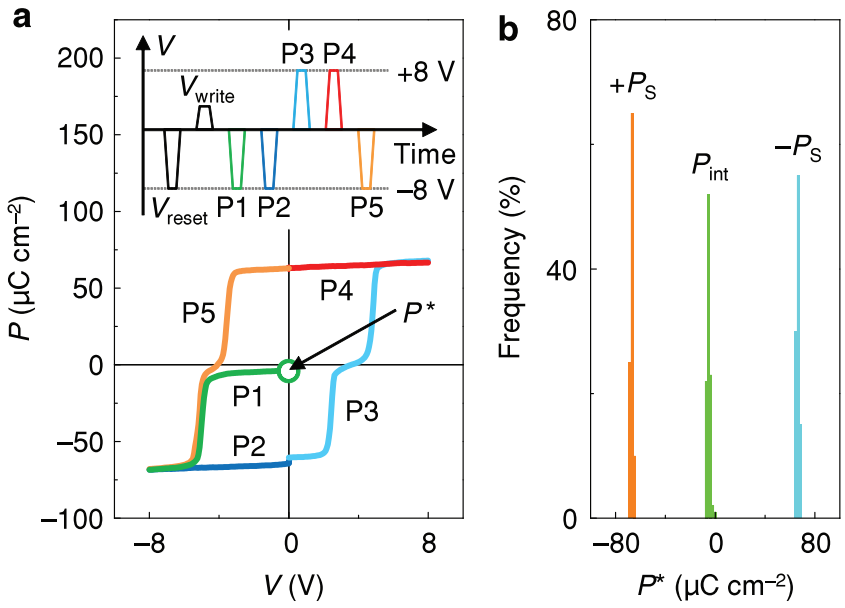

Figure 4. Demonstration of a reproducible tri-state nonvolatile memory. a) P–V hysteresis loop measured by applying trapezoid pulses (inset). We wrote the $+P_S$, P_{int}, and $-P_S$ states by applying –8 V, 3 V, and +8 V, respectively. Then, we measured the actual values of the polarization states, denoted by P^*, by a pulse measurement of the hysteresis. b) Plot of frequency versus measured P^* for the double P–V hysteresis loop, obtained by 200 pulse measurements for each polarization state.

Our defect-engineering concept will be useful in devising novel ferroelectric devices. As an example, we applied our concept to tri-state nonvolatile memory. As seen in PFM and in P–V loop studies, it is clear that we can make at least three stable polarization states, that is, $-P_S$, P_{int}, and $+P_S$. When each ferroelectric memory cell has three stable polarization states, nine states (3×3) can be programmed using two memory cells. If eight of the nine possible states are employed, then two memory cells can work as the three cells of traditional binary memory. Thus, compared with conventional bistable data storage using $-P_S$ and $+P_S$ states only, tri-state data storage can enhance the memory density by 50%.[31]

One requirement for the memory state is state reproducibility. We checked the reproducibility of the P_{int} state using a pulse hysteresis measurement,[32] as depicted in the inset of **Figure 4**a. We repeated this read–write process for 200 cycles. Even for 200 cycles, the P_{int} state showed a narrow distribution, with a mean value of –5.3 μC cm^{-2} and standard deviation of 1.4 μC cm^{-2} (Figure 4b). Similarly, we checked the reproducibility of the $-P_S$ and $+P_S$ states. Our results confirmed that the reproducibility of the tristable states is good.

We have demonstrated that the influence of D_{defect} is revealed as distinct double-polarization switching. Our results, however, did not limit the effect of D_{defect} by double-polarization switching; it is possible to further tune this process. For example, we might make a triple P–V loop by combining the portion and density control of aligned D_{defect}. This scheme is summarized in the Supporting Information, Figure S5. If triple or multiple P–V loops are realized, then we can further enhance the functionality of ferroelectric devices, such as high-density data storage of ferroelectric memories.

Our study also provided general insight into the active engineering of defects in ferroelectrics. Despite recent interest in the defect effects in ferroelectrics,[12–16] efforts to use defects in the active control of ferroelectric properties have been limited. Most studies have used as-grown ferroelectrics, in which the defects were already present, or long-aging processes to achieve the required defect structure. However, our work proposes that D_{defect} can be engineered actively and systematically using a simple procedure of partial domain writing and subsequent annealing. Additionally, our approach can be extended to studies on the contribution of D_{defect} to various phenomena in ferroelectric and multiferroic materials.

Last, we suggest that the stability of D_{defect} can be strengthened by proper metal doping. We found that the D_{defect} effect in the film could be stable for up to 10^4 cycles of P–V loop measurements, after which its effect became weakened.[19] For practical applications, D_{defect} and its corresponding alignment need to be more stable against the repeated electrical stress. Intentional metal doping is an effective way to enhance the stability of D_{defect}, which depends strongly on which metal impurity associates with the oxygen vacancy.[33] For example, the binding energy of D_{defect} can be increased significantly by a proper choice of metal impurity. In our study, however, we did not intentionally introduce any defect (e.g., metal doping). The D_{defect} is expected to consist of Bi vacancy (or a metal impurity) and an oxygen vacancy, which naturally exists in our samples (Supporting Information, Figure S6–8). Thus, future studies on D_{defect} with intentional metal doping will be important to enhance the D_{defect} stability and its applicability.

In summary, we directly demonstrated the effect of D_{defect} on polarization switching in ferroelectric materials. Partial domain writing followed by thermal annealing enabled us to actively control the defect structure and the associated polarization switching. We visualized the defect-mediated polarization switching using local PFM measurements. Additionally, we successfully demonstrated that P–V loops were systematically varied according to the D_{defect} structure. The observed close correlation between defect structure and polarization switching would provide a platform for advancing new applications in ferroelectric materials, such as high-density multilevel data storage.

Experimental Section

Sample Fabrication: We used pulsed laser ablation to grow 200-nm-thick $BiFeO_3$ epitaxial thin films on $SrTiO_3$ (001) single-crystal substrates with a 4° miscut toward the [100] direction. For the lattice-matched bottom electrodes on the $SrTiO_3$ substrates, we used epitaxially strained $SrRuO_3$ films. We deposited the $SrRuO_3$ layer by ablating the stoichiometric $SrRuO_3$ ceramic target using a KrF excimer laser (248 nm, Lambda Physik) with a repetition rate of 2 Hz. Then, we deposited $BiFeO_3$ film by ablating the stoichiometric $BiFeO_3$ ceramic target with a repetition rate of 5 Hz. During deposition, we kept the substrate temperature at 570 °C and maintained the chamber oxygen partial pressure at 100 mTorr. We deposited 40-nm-thick Pt at room temperature by sputtering and patterned the top electrode by photolithography. We confirmed good crystalline quality of every film using four-circle high-resolution X-ray diffractometry (XRD) (D8 Advance, Bruker AXS) and atomic force microscopy (AFM) (XE-100, Park Systems) (Supporting Information, Figure S1). Note that, in addition to the films grown by pulsed laser deposition, we also used other $BiFeO_3$ films grown by a sputter deposition.[34,35] For the latter films, we obtained nearly the same results on polarization switching changes, controlled by the D_{defect} alignment.

Ferroelectric Domain Imaging: We used a PFM (XE-100, Park Systems) to write a local domain and investigate domain evolution under the influence of D_{defect}. We performed PFM measurements at room temperature with commercially available Pt/Ir-coated Si tips (PPP-EFM, Nanosensors). With conductive AFM tips, it was possible to measure local electrical and topographical properties both simultaneously and independently. For PFM imaging, we applied an AC voltage of 1.0 V_{rms} at 17.1 kHz to the bottom electrode (i.e., sample bias). We measured the amplitude and phase signals of the converse piezoelectric responses with a lock-in amplifier (SR830, Stanford Research Systems).

P–V Hysteresis Loops: We investigated the ferroelectric properties of $BiFeO_3$ films using a T-F analyzer (aixACCT) and a low-temperature probe station (Desert Cryogenics). We measured the P–V hysteresis loops at 2 kHz. The measurement temperatures for Figure 3c,d were 150 K and room temperature, respectively. We performed pulse measurements of polarization hysteresis using trapezoid pulses at 150 K (Figure 4a), with pulse duration of 2 ms and a pulse delay of 0.2 s. To obtain the statistical distribution of the tristable polarization states (Figure 4b), we repeated the read–write process 200 times for each state.

Supporting Information

Supporting Information is available from the Wiley Online Library or from author.

Acknowledgements

This work was supported by the Institute of Basic Science (IBS) and the National Research Foundation of Korea (NRF) (Grant No. 2012-0005847; J.-G.Y.: No. 2011-0005145) grant funded by the Korea government (MEST). The work at the University of Wisconsin–Madison was supported by the Army Research Office through grant W911NF-10-1-0362, the National Science Foundation through Grant No. ECCS-0708759, and a David & Lucile Packard Fellowship (C.B.E.). D.L. acknowledges support from the POSCO TJ Park Doctoral Foundation.

Received: July 30, 2012
Revised: September 5, 2012
Published online: October 1, 2012

[1] J. F. Scott, *Science* **2007**, *315*, 954.
[2] J. F. Scott, C. A. P. De Araujo, *Science* **1989**, *246*, 1400.
[3] M. E. Lines, A. M. Glass, *Principles and Applications of Ferroelectrics and Related Materials*, Clarendon, Oxford **1977**.
[4] M. Dawber, K. M. Rabe, J. F. Scott, *Rev. Mod. Phys.* **2005**, *77*, 1083.
[5] V. Garcia, S. Fusil, K. Bouzehouane, S. Enouz-Vedrenne, N. D. Mathur, A. Barthelemy, M. Bibes, *Nature* **2009**, *460*, 81.
[6] V. Garcia, M. Bibes, L. Bocher, S. Valencia, F. Kronast, A. Crassous, X. Moya, S. Enouz-Vedrenne, A. Gloter, D. Imhoff, C. Deranlot, N. D. Mathur, S. Fusil, K. Bouzehouane, A. Barthélémy, *Science* **2010**, *327*, 1106.
[7] P. Maksymovych, S. Jesse, P. Yu, R. Ramesh, A. P. Baddorf, S. V. Kalinin, *Science* **2009**, *324*, 1421.
[8] H. Zheng, J. Wang, S. E. Lofland, Z. Ma, L. Mohaddes-Ardabili, T. Zhao, L. Salamanca-Riba, S. R. Shinde, S. B. Ogale, F. Bai, D. Viehland, Y. Jia, D. G. Schlom, M. Wuttig, A. Roytburd, R. Ramesh, *Science* **2004**, *303*, 661.
[9] Y.-H. Chu, L. W. Martin, M. B. Holcomb, M. Gajek, S.-J. Han, Q. He, N. Balke, C.-H. Yang, D. Lee, W. Hu, Q. Zhan, P.-L. Yang, A. Fraile-Rodríguez, A. Scholl, S. X. Wang, R. Ramesh, *Nat. Mater.* **2008**, *7*, 478.
[10] T. Choi, S. Lee, Y. J. Choi, V. Kiryukhin, S.-W. Cheong, *Science* **2009**, *324*, 63.
[11] D. Li, M. H. Zhao, J. Garra, A. M. Kolpak, A. M. Rappe, D. A. Bonnell, J. M. Vohs, *Nat. Mater.* **2008**, *7*, 473.
[12] S. Jesse, B. J. Rodriguez, S. Choudhury, A. P. Baddorf, I. Vrejoiu, D. Hesse, M. Alexe, E. A. Eliseev, A. N. Morozovska, J. Zhang, L.-Q. Chen, S. V. Kalinin, *Nat. Mater.* **2008**, *7*, 209.
[13] P. Maksymovych, N. Balke, S. Jesse, M. Huijben, R. Ramesh, A. P. Baddorf, S. V. Kalinin, *J. Mater. Sci.* **2009**, *44*, 5095.
[14] C. T. Nelson, P. Gao, J. R. Jokisaari, C. Heikes, C. Adamo, A. Melville, S.-H. Baek, C. M. Folkman, B. Winchester, Y. Gu, Y. Liu, K. Zhang, E. Wang, J. Li, L.-Q. Chen, C.-B. Eom, D. G. Schlom, X. Pan, *Science* **2011**, *334*, 968.
[15] P. Gao, C. T. Nelson, J. R. Jokisaari, S.-H. Baek, C. W. Bark, Y. Zhang, E. Wang, D. G. Schlom, C.-B. Eom, X. Pan, *Nat. Commun.* **2011**, *2*, 591.
[16] X. B. Ren, *Nat. Mater.* **2004**, *3*, 91.
[17] W. L. Warren, D. Dimos, G. E. Pike, B. A. Tuttle, M. V. Raymond, R. Ramesh, J. T. Evans, *Appl. Phys. Lett.* **1995**, *67*, 866.
[18] G. Arlt, H. Neumann, *Ferroelectrics* **1988**, *87*, 109.
[19] C. M. Folkman, S. H. Baek, C. T. Nelson, H. W. Jang, T. Tybell, X. Q. Pan, C. B. Eom, *Appl. Phys. Lett.* **2010**, *96*, 052903.
[20] D. Lee, A. Yoon, S. Y. Jang, J.-G. Yoon, J.-S. Chung, M. Kim, J. F. Scott, T. W. Noh, *Phys. Rev. Lett.* **2011**, *107*, 057602.
[21] R. Metselaar, P. K. Larsen, *J. Phys. Chem. Solids* **1976**, *37*, 599.
[22] L. Chen, X. M. Xiong, H. Meng, P. Lv, J. X. Zhang, *Appl. Phys. Lett.* **2006**, *89*, 071916.
[23] J. Wang, J. B. Neaton, H. Zheng, V. Nagarajan, S. B. Ogale, B. Liu, D. Viehland, V. Vaithyanathan, D. G. Schlom, U. V. Waghmare, N. A. Spaldin, K. M. Rabe, M. Wuttig, R. Ramesh, *Science* **2003**, *299*, 1719.
[24] G. Catalan, J. F. Scott, *Adv. Mater.* **2009**, *21*, 2463.

[25] P. Paruch, J.-M. Triscone, *Appl. Phys. Lett.* **2006**, *88*, 162907.
[26] S. V. Kalinin, D. A. Bonnell, *Phys. Rev. B* **2002**, *65*, 125408.
[27] D. J. Kim, J. Y. Jo, T. H. Kim, S. M. Yang, B. Chen, Y. S. Kim, T. W. Noh, *Appl. Phys. Lett.* **2007**, *91*, 132903.
[28] A. Gruverman, D. Wu, J. F. Scott, *Phys. Rev. Lett.* **2008**, *100*, 097601.
[29] D. Lee, S. M. Yang, T. H. Kim, B. C. Jeon, Y. S. Kim, J.-G. Yoon, H. N. Lee, S. H. Baek, C. B. Eom, T. W. Noh, *Adv. Mater.* **2012**, *24*, 402.
[30] V. Garcia, M. Bibes, *Nature* **2012**, *483*, 279.
[31] K. R. Raiter, B. F. Cockburn, *Proceedings of the IEEE International Workshop on Memory Technology, Design, and Testing*, IEEE Computer Society Press, USA **2005**.
[32] H. N. Lee, S. M. Nakhmanson, M. F. Chisholm, H. M. Christen, K. M. Rabe, D. Vanderbilt, *Phys. Rev. Lett.* **2007**, *98*, 217602.
[33] P. Erhart, R.-A. Eichel, P. Träskelin, K. Albe, *Phys. Rev. B* **2007**, *76*, 174116.
[34] H. W. Jang, D. Ortiz, S. H. Baek, C. M. Folkman, R. R. Das, P. Shafer, Y. Chen, C. T. Nelson, X. Pan, R. Ramesh, C. B. Eom, *Adv. Mater.* **2009**, *21*, 817.
[35] S. H. Baek, H. W. Jang, C. M. Folkman, Y. L. Li, B. Winchester, J. X. Zhang, Q. He, Y. H. Chu, C. T. Nelson, M. S. Rzchowski, X. Q. Pan, R. Ramesh, L. Q. Chen, C. B. Eom, *Nat. Mater.* **2010**, *9*, 309.